Supplementary Information

Single molecule SERS and detection of biomolecules with a single gold nanoparticle on mirror junction

Li Li,[a,c] Tanya Hutter,[b] Ullrich Steiner[c] and Sumeet Mahajan*[a,c]

[a] *Institute for Life Sciences, Highfield Campus, University of Southampton, SO17 1BJ, UK. E-mail: S.Mahajan@soton.ac.uk*
[b] *Department of Chemistry, University of Cambridge, Lensfield Road, Cambridge, CB2 1EW, UK.*
[c] *Department of Physics, Cavendish Laboratory, University of Cambridge, Cambridge, CB3 0HE, UK.*

Experimental Methods

Fabrication of the Au nanosphere on Au thin film (AuNS-AuTF) configuration with various probe molecules: The AuTF was fabricated by thermal evaporation using a BOC Edwards Auto 306 resistance evaporator at 10^{-6} mbar. Specifically, a 5 nm layer was first deposited onto a clean Si wafer, followed by the deposition of an approximately 80 nm thick Au layer. In the thin film (TF)-functionalization approach, the pre-cut Au substrate (approximately 5 mm × 5 mm) was immersed in the following solutions for 1 hr to overnight to allow for the formation of a monolayer of probe molecules, unless otherwise specified. The following solutions were used: 1 mM solution of 4,4′-dimercaptostilbene (dithiol, >96%, Aldrich) in tetrahydrofuran (THF); 1 mM aqueous solutions of L-glutathione (GSH, BioXtra, ≥ 98%, Sigma-Aldrich) and phenylalanine (PHE, 99%, Lancaster); 250 μM aqueous solution of L-tyrosine (TYR, BioUltra, ≥ 99.0%, Sigma). The Au substrates were subsequently rinsed with the corresponding solvents (THF or DI water) to remove excess probe molecules from the surface. Then a drop (~20 μL) of AuNSs (average diameter of 100 nm, BBI life sciences) was cast onto molecule-functionalized AuTF for a few minutes, followed by rinsing and air-drying to remove unattached AuNSs. For the detection of adenine using the nanoparticle (NP)-functionalization approach, AuNS solution with a concentration of 0.0093 nM was incubated with a solution containing adenine (≥ 99%, Sigma) at different concentrations (100 μM ~ 10 nM). The mixed solution was stirred for overnight and then the adenine-functionalized AuNSs were separated *via* centrifugation and redispersed in DI water. Then a drop (~20 μL) of these AuNSs was cast onto AuTF, followed the same treatment described above. For the detection of

Oxytocin (OT, Sigma-Aldrich) using the TF-functionalization approach, it was first dissolved in citric buffer solution (pH = 4.6, 0.1 M) at a concentration of 1 mM, and tris(2-carboxyethyl)phosphine hydrochloride (Aldrich) was subsequently added to reach a concentration of approximately 5 mM. The mixed solution was aged for 1−2 hrs in order to activate the disulfide group, and then diluted to 250 µM in PBS solution (Source BioScience), into which the Au substrate was immersed for 2−4 days. In the NP-functionalization approach, 70 µL of OT 1 mM aqueous solution was mixed with 500 µL of 100 nm AuNSs with a concentration of 0.0093 nM. After stirring overnight, the OT-functionalized AuNSs were separated *via* centrifugation and redispersed in DI water. The samples in both cases were fabricated similarly as described above.

SM-SERS detection using bianalyte method: AuNS solution with a concentration of 0.0093 nM was incubated with a solution containing both methylene blue (MB, BDH chemical Ltd.) and rhodamine 6G (R6G, 98%, Sigma) at a concentration of 4 nM and 0.2 nM, respectively. The mixed solution was stirred for 2 hrs and then the dye-functionalized AuNSs were separated *via* centrifugation and redispersed in DI water. Then a drop (~20 µL) of these AuNSs was cast onto clean AuTF which was followed by rinsing and air-drying.

Calculation of the SERS EF[1]: The SERS EF of AuNS-dithiol-AuTF in Fig. 1c was estimated by comparing the intensities of the 8b band of the unenhanced Raman scattering (I_{Raman}) from a 5 mM THF solution of dithiol, obtained by focusing the laser light into a quartz cuvette, and the corresponding enhanced Raman scattering (ERS) signals (I_{ERS}) obtained from the AuNS-dithiol-AuTF system. The detection volume of the solution-phase dithiol sample (V_f) was calculated using the equation V_f = (depth of focus)^2 × (focus area) = $(1.4n\lambda/NA^2) \times \pi(0.4\lambda/2NA)^2$. The surface density of the adsorbed dithiol molecules on the Au surface and the number density of the dithiol molecules in solution are ρ_s = 3.3 molecules/nm^2, and ρ_v = 3 × 10^{-3} molecules/nm^3, respectively. The enhanced area (A) is taken as the area on the Au substrate that experiences a local field enhancement $|E/E_0|^4$ larger than $1/2|E_{max}/E_0|^4$, where E_{max} is the maximum local-field amplitude. The EF of the AuNS-dithiol-AuTF system was obtained by comparing the unenhanced Raman signal from a single dithiol molecule with the ERS signal from a single dithiol molecule sandwiched

between the AuNS and the Au surface, using the relationship, EF = $[I_{ERS}/(\rho_s A)]/[I_{Raman}/(\rho_v V_f)]$. The length of dithiol is taken as 1.3 nm.[2]

Simulations: A two-dimensional model using COMSOL Multiphysics v4.2 was constructed. The simulation was performed in two steps: the first step is for the substrate only, using Floquet boundary conditions combined with a port-boundary for the field excitation. The second step was solved for the scattered field due to the AuNS on the substrate. Perfectly matched layers were used at the boundary to absorb the scattered radiation in all directions, particularly to prevent scattering artifacts from edges. The *p*-polarized light at an incident angle of 45° to the surface normal was used. The simulations were performed for wavelengths in the range 375−1000 nm. The complex refractive index of Au as a function of wavelength was taken from the literature.[3]

Characterization: Raman spectra were acquired using a Renishaw inVia Raman system equipped with an integral microscope. An objective with the magnification of 100× (Leica, NA: 0.85) was used. Lasers with wavelength of 532 nm, 633 nm and 785 nm were used as the excitation sources typically at powers <1 mW. Scanning electron microscope imaging was performed using a LEO 1530 VP microscope.

Table S1 Simulated $|E_{ymax}(ex)/E_0|$ and $|E_{ymax}(sc)/E_0|$ for the excitations at 532, 633 and 785 nm and at an angle of incidence of 45°. (The outgoing wavelengths are calculated based on the vibration mode at 1581 cm^{-1}).

	$|E_{ymax}/E_0|$	$|E_{ymax}(ex)/E_0|^2 \times |E_{ymax}(sc)/E_0|^2$
532 nm (ex)	15.89	290852
581 nm (sc)	33.94	
633 nm (ex)	40.60	1518341
703 nm (sc)	30.35	
785 nm (ex)	21.40	134226
896 nm (sc)	17.12	

Table S2 The event distribution in the case of two molecules residing in the enhanced area. A and B represent two types of molecules, O represents the null case.

	Possible combinations	Percentage of events
Event A	AA, AO, OA	37.5%
Event B	BB, BO, OB	37.5%
Mixed event	AB, BA	25%
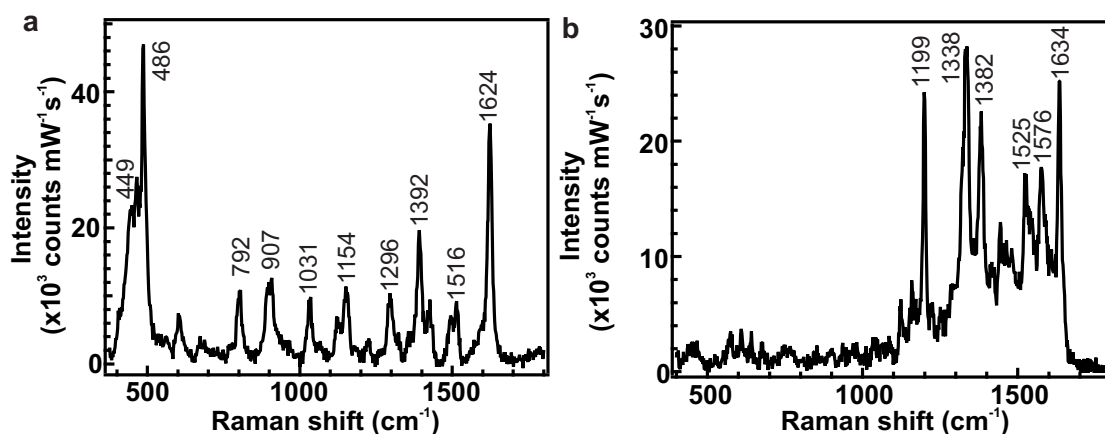
Fig. S1 The SERS spectra of (a) MB and (b) R6G acquired *via* the TF-functionalization approach. The backgrounds have been subtracted.
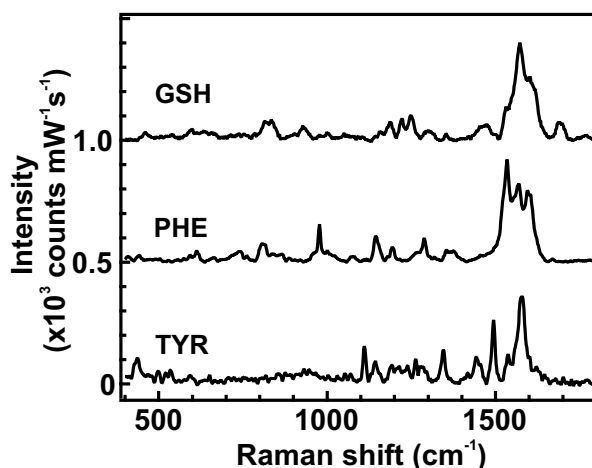
Fig. S2 The SERS spectra of probing GSH, PHE and TYR *via* the TF-functionalization approach. The backgrounds have been subtracted.

Peak assignments

Approximate description of the modes

ν, stretch; b, bend; δ, in-plane bend; γ, out-of-plane bend; π, wagging; τ, torsion; β, deformation, r, rock; tw, twist; s, scissor. For ring vibrations, the corresponding vibrational modes of benzene and the symmetry species under C_{2v} symmetry are indicated.

Assignments of MB in Fig. 3c[4]

Raman shift (cm^{-1})	Assignments
443	δ(CNC)
484	δ(CSC)
1320	ν(CN)
1390	ν(CN)
1477	δ(NH$_2$)
1527	δ(NH$_2$)
1628	ν_{ring}(CC)

Assignments of R6G in Fig. 3e[5]

Raman shift (cm^{-1})	Assignments
1175	b(CH)
1516	ν(CC)
1558	ν(CO)
1610	ν(CC)
1640	ν(CC)

Assignments of GSH in Fig. S2[6]

Raman shift (cm^{-1})	Assignments
814	ν(NC), r(CH$_2$)
836	b(COH), β(NCC)
929	b(CSH), r(CH$_2$), ν(NC)
1187	b(CH), w(CH$_2$), ν(NC)
1221	tw(CH$_2$)
1250	w(CH$_2$), b(CH), tw(CH$_2$)
1452	b(CH$_2$)
1531	δ(NH), ν(NC), ν(CC)
1571	δ(NH), ν(NC), ν(CC), δ(CO)
1600	ν_{asym}(COO), r(COO)
1693	ν(CO), β(CCO)

Assignments of PHE in Fig. S2[7,8]

Raman shift (cm^{-1})	Assignments
977	ν(C–COO)
1001	γ(CC)+γ(CCC), 18a$_1$
1145	δ(CH), 9b$_2$, ν_{asym}(CCN)
1194	δ(CH), 9a$_1$, r(NH$_3^+$)
1263, 1288	tw(CH$_2$)

1533	$\beta_{sym}(NH_3^+)$
1569	$\nu(CC)$, $8b_2$, $\nu_{asym}(COO)$, $\beta_{sym}(NH_3^+)$
1601	$\nu(CC)$, $8a_1$, $\nu_{asym}(COO)$, $\beta_{sym}(NH_3^+)$

Assignments of TYR in Fig. S2[7,8]

Raman shift (cm^{-1})	Assignments
1111	$r(NH_3^+)$
1143	$\delta(CH)$, $9b_2$, $\nu_{asym}(CCN)$
1191, 1214	$\delta(CH)$, $9a_1$, $r(NH_3^+)$
1239	$\beta(COH)$
1263, 1285	$\nu(COH)$, $tw(CH_2)$
1345	$\nu(CN)$, $\delta(CH)$
1442	$\nu(CC)+\delta(CH)$, $19b_2$, $\nu(NH_3^+)$
1494	$\nu(CC)+\delta(CH)$, $19a_1$, $s(CH_2)$
1536	$\nu_{asym}(CO)$, $\nu_{sym}(C=C)$, $\beta_{sym}(NH_3^+)$
1577	$\nu(CC)$, $8b_2$, $\nu_{asym}(COO)$, $\beta_{sym}(NH_3^+)$
1621	$\nu(C=C)$, $\beta_{asym}(NH_3^+)$

Assignments of OT in Fig. 4a[8,9]

Raman shift (cm^{-1})	Assignments
1136, 1169	$\delta(CH)$, $9b_2$, $\nu_{asym}(CCN)$
1204, 1220	$\delta(CH)$, $9a_1$, $r(NH_3^+)$
1263	$\nu(COH)$, $tw(CH_2)$, $\delta(CC\alpha H)$
1336, 1375	$\nu(CN)$, $\delta(CH)$
1411	$\delta(CH_2)$
1484	$\nu(CC)+\delta(CH)$, $19a_1$, $s(CH_2)$
1534	$\nu_{asym}(CO)$, $\nu_{sym}(C=C)$, $\beta_{sym}(NH_3^+)$
1575	$\nu(CC)$, $8b_2$, $\beta_{sym}(NH_3^+)$
1618	$\nu(C=C)$, $\beta_{asym}(NH_3^+)$
1660	amide I random coil

Assignments of OT in Fig. 4b[8,9]

Raman shift (cm^{-1})	Assignments
493	$\nu(SS)$ GGG
523	$\nu(SS)$ TGG
553	$\nu(SS)$ TGT
727	$\nu(CS)$ Pc-T
794	$\nu_{asym}(CSC)$
813, 847	Tyr Fermi doublet
986	$\nu(CC)$
1020	$\nu(CN)$
1167	$\delta(CH)$, $9b_2$, $\nu_{asym}(CCN)$
1242	amide III random coil
1263	$\nu(COH)$, $tw(CH_2)$, $\delta(CC\alpha H)$
1319	$w(CH_2)$
1370	$\nu(CN)$, $\delta(CH)$
1497	$\nu(CC)+\delta(CH)$, $19a_1$, $s(CH_2)$
1529, 1555	$\nu_{asym}(CO)$, $\nu_{sym}(C=C)$, $\beta_{sym}(NH_3^+)$

1582	$v(CC)$, $8b_2$, $\beta_{sym}(NH_3^+)$
1619	$v(C=C)$, $\beta_{asym}(NH_3^+)$
1653	amide I random coil

1582	$v(CC)$, $8b_2$, $\beta_{sym}(NH_3^+)$
1619	$v(C=C)$, $\beta_{asym}(NH_3^+)$
1653	amide I random coil

References:

1   W.-H. Park and Z. H. Kim, *Nano Lett.*, 2010, **10**, 4040-4048.
2   N. Guarrotxena, Y. Ren and A. Mikhailovsky, *Langmuir*, 2011, **27**, 347-351.
3   P. B. Johnson and R. W. Christy, *Phys. Rev. B*, 1972, **6**, 4370-4379.
4   K. Hutchinson, R. E. Hester, W. J. Albery and A. R. Hillman, *J. Chem. Soc., Faraday Trans. 1*, 1984, **80**, 2053-2071.
5   Y. Q. Wang, S. Ma, Q. Q. Yang and X. j. Li, *Appl. Surf. Sci.*, 2012, **258**, 5881-5885.
6   W. Qian and S. Krimm, *Biopolymers*, 1994, **34**, 1377-1394.
7   M. Osawa, N. Matsuda, K. Yoshii and I. Uchida, *J. Phys. Chem.*, 1994, **98**, 12702-12707.
8   T. Deckert-Gaudig, E. Rauls and V. Deckert, *J. Phys. Chem. C*, 2010, **114**, 7412-7420.
9   E. Podstawka, Y. Ozaki and L. M. Proniewicz, *Appl. Spectrosc.*, 2004, **58**, 1147-1156.